Wafer-scale broadband antireflective silicon fabricated by metal-assisted chemical etching using spin-coating Ag ink

Chan Il Yeo,[1] Young Min Song,[1] Sung Jun Jang,[1] and Yong Tak Lee[1,2,3]*

[1]*School of Information and Communications, Gwangju Institute of Science and Technology, 1 Oryong-dong, Buk-gu, Gwangju, 500-712, Korea*
[2]*Graduate Program of Photonics and Applied Physics, Gwangju Institute of Science and Technology, 1 Oryong-dong, Buk-gu, Gwangju, 500-712, Korea*
[3]*Department of Nanobio Electronics and Materials, Gwangju Institute of Science and Technology,1 Oryong-dong, Buk-gu, Gwangju, 500-712, Korea*
ytlee@gist.ac.kr

Abstract: We report broadband antireflective disordered subwavelength structures (d-SWSs), which were fabricated on 4-inch silicon wafers by spin-coating Ag ink and metal-assisted chemical etching. The antireflection properties of the d-SWSs depend on its dimensions and heights, which were changed by the sintering temperature of the spin-coated Ag ink and etching time. The fabricated d-SWSs drastically reduced surface reflection over a wide range of wavelengths and incident angles, providing good surface uniformity. The d-SWSs with the most appropriate geometry for practical solar cell applications exhibit only 1.23% solar-weighted reflectance in the wavelength range of 300-1100 nm and average reflectance <5% up to an incident angle of 55° in the wavelength range of 300-2500 nm. This simple and low-cost nanofabrication method for antireflection could be of great importance in optical device applications because it allows mass production without any lithography processes or sophisticated equipment.

OCIS codes: (220.4241) Nanostructure fabrication; (310.6628) Subwavelength structure; (160.4760) Optical properties; (040.5350) Photovoltaic.

References and links

1. J. A. Turner, "A realizable renewable energy future," Science **285**(5428), 687–689 (1999).
2. A. Shah, P. Torres, R. Tscharner, N. Wyrsch, and H. Keppner, "Photovoltaic technology: the case for thin-film solar cells," Science **285**(5428), 692–698 (1999).
3. S. A. Boden and D. M. Bagnall, "Tunable reflection minima of nanostructured antireflective surfaces," Appl. Phys. Lett. **93**(13), 133108 (2008).
4. Y. M. Song, J. S. Yu, and Y. T. Lee, "Antireflective submicrometer gratings on thin-film silicon solar cells for light-absorption enhancement," Opt. Lett. **35**(3), 276–278 (2010).
5. Z. Yu, H. Gao, W. Wu, H. Ge, and S. Y. Chou, "Fabrication of large area subwavelength antireflection structures on Si using trilayer resist nanoimprint lithography and liftoff," J. Vac. Sci. Technol. B **21**(6), 2874–2877 (2003).
6. J. Tommila, V. Polojärvi, A. Aho, A. Tukiainen, J. Viheriälä, J. Salmi, A. Schramm, J. M. Kontio, A. Turtiainen, T. Niemi, and M. Guina, "Nanostructured broadband antireflection coatings on AlInP fabricated by nanoimprint lithography," Sol. Energy Mater. Sol. Cells **94**(10), 1845–1848 (2010).
7. H. Sai, H. Fujii, K. Arafune, Y. Ohshita, M. Yamaguchi, Y. Kanamori, and H. Yugami, "Antireflective subwavelength structures on crystalline Si fabricated using directly formed anodic porous alumina masks," Appl. Phys. Lett. **88**(20), 201116 (2006).
8. S. Wang, X. Z. Yu, and H. T. Fan, "Simple lithographic approach for subwavelength structure antireflection," Appl. Phys. Lett. **91**(6), 061105 (2007).
9. C. H. Chiu, P. Yu, H. C. Kuo, C. C. Chen, T. C. Lu, S. C. Wang, S. H. Hsu, Y. J. Cheng, and Y. C. Chang, "Broadband and omnidirectional antireflection employing disordered GaN nanopillars," Opt. Express **16**(12), 8748–8754 (2008).
10. Y. Lee, K. Koh, H. Na, K. Kim, J.-J. Kang, and J. Kim, "Lithography-free fabrication of large area subwavelength antireflection structures using thermally dewetted Pt/Pd alloy etch mask," Nanoscale Res. Lett. **4**(4), 364–370 (2009).

#149230 - $15.00 USD Received 14 Jun 2011; accepted 30 Jun 2011; published 2 Aug 2011

11. Y. M. Song, G. C. Park, S. J. Jang, J. H. Ha, J. S. Yu, and Y. T. Lee, "Multifunctional light escaping architecture inspired by compound eye surface structures: From understanding to experimental demonstration," Opt. Express **19**(S2 Suppl 2), A157–A165 (2011).
12. Y. M. Song, E. S. Choi, G. C. Park, C. Y. Park, S. J. Jang, and Y. T. Lee, "Disordered antireflective nanostructures on GaN-based light-emitting diodes using Ag nanoparticles for improved light extraction efficiency," Appl. Phys. Lett. **97**(9), 093110 (2010).
13. K. Q. Peng, J. J. Hu, Y. J. Yan, Y. Wu, H. Fang, Y. Xu, S. T. Lee, and J. Zhu, "Fabrication of single-crystalline silicon nanowires by scratching a silicon surface with catalytic metal particles," Adv. Funct. Mater. **16**(3), 387–394 (2006).
14. C. Chartier, S. Bastide, and C. Lévy-Clément, "Metal-assisted chemical etching of silicon in HF-H_2O_2," Electrochim. Acta **53**(17), 5509–5516 (2008).
15. M.-L. Zhang, K.-Q. Peng, X. Fan, J.-S. Jie, R.-Q. Zhang, S.-T. Lee, and N.-B. Wong, "Preparation of large-area uniform silicon nanowires arrays through metal-assisted chemical etching," J. Phys. Chem. C **112**(12), 4444–4450 (2008).
16. H. Sai, Y. Kanamori, K. Arafune, Y. Ohshita, and M. Yamaguchi, "Light trapping effect of submicron surface textures in crystalline Si solar cells," Prog. Photovolt. Res. Appl. **15**(5), 415–423 (2007).
17. Web site for NREL's AM1.5 Standard Dataset: *http://rredc.nrel.gov/solar/spectra/am1.5/*.
18. Y. Yasukawa, H. Asoh, and S. Ono, "Site-selective chemical etching of GaAs through a combination of self-organized spheres and silver particles as etching catalyst," Electrochem. Commun. **10**(5), 757–760 (2008).
19. X. Li, Y.-W. Kim, P. W. Bohn, and I. Adesida, "In-plane bandgap control in porous GaN through electroless wet chemical etching," Appl. Phys. Lett. **80**(6), 980–982 (2002).

1. Introduction

Over recent years, there has been an increasing demand for high-efficiency photovoltaic devices, which are key components in solving global-warming issues due to burning fossil fuels [1,2]. Because the conversion efficiency of a solar cell depends on its photon absorption, developing a broadband and omnidirectional antireflective structure is indispensable for improving the performance of solar cells [3–11]. Subwavelength structures (SWSs) are the most appropriate type of antireflective structure for improving the performance of optical and optoelectronic devices including solar cells, photodetectors, and displays. A great deal of effort has been made to produce SWSs in various ways. Common methods of SWSs fabrication are based on dry etching of nano-scale mask patterns formed by e-beam/interference/nanoimprint lithography [3–6] or anodic porous alumina mask [7]. However, these methods are expensive, complex, and not adequate for a wafer-scale process. Recently, disordered SWSs (d-SWSs) fabricated by nonlithographic metal nanoparticle and dry etching methods have been reported to overcome these obstacles [8–12]. Unfortunately, this fabrication method still has noneconomic barriers such as long process time and the necessity of vacuum systems for metal evaporation, thermal dewetting, and dry etching. These problems restrict the employment of SWSs in practical solar cell applications. To address these problems, an economical and simple nanofabrication technique is required.

We report wafer-scale broadband antireflective silicon fabricated by a nanofabrication method that uses spin-coated Ag ink and metal-assisted chemical etching based on the strong catalytic activity of metal [13–15] to produce silicon d-SWSs. This simple, fast, and cost-effective wafer-scale process allows mass production without any lithography processes or sophisticated equipment. To achieve desirable antireflective d-SWSs for practical solar cell applications, d-SWSs with various dimensions and heights were fabricated and their antireflection properties were systematically investigated. The fabricated d-SWSs on 4-inch silicon wafer significantly reduced surface reflection over a wide range of incident angles and wavelengths, in comparison to bare silicon and showed good surface uniformity.

2. Fabrication of wafer-scale antireflective silicon

Figure 1 shows a schematic illustration of the process steps for fabricating the d-SWSs by spin-coating Ag ink and metal-assisted chemical etching. Scanning electron microscope (SEM) images from each process step are also shown in the right column of Fig. 1. A diluted solvent-based Ag ink, which is composed of soluble Ag clusters that includes Ag atoms of 10% wt., was spin-coated on p-type crystalline silicon (100) wafers (Boron-doped with resistivity of 1-30 Ω cm). To obtain the optimum thickness of the as-coated Ag layer, the dilution ratio of 1:2 (Ag ink: isopropanol) and coating conditions were adjusted. The wafers

#149230 - $15.00 USD Received 14 Jun 2011; accepted 30 Jun 2011; published 2 Aug 2011

were sintered on a hotplate at temperatures of 150°C, 170°C, 200°C, and 250°C for 3 min, to produce nano-scale Ag mesh structures with various dimensions. In this method, the thermal treatment temperatures were much lower than the previously reported methods, in which the solid metal films were used to form metal nanoparticles for dry etching [9–12]. Thus, device degradation problems due to higher thermal temperatures may be addressed by the application of this method. At the initial state of the sintering process, the solvent in the Ag ink was evaporated. As the sintering time increased, the nano-scale random Ag mesh structures were formed by self-agglomeration of Ag due to the enhanced surface energy of Ag [10]. To generate d-SWSs, the wafers were immersed in an aqueous solution of 70% nitric acid, 50% hydrofluoric acid, and deionized (DI) water (4:1:20 v/v/v) at room temperature. The solution was deliberately mixed because it affects the etch rate and surface morphology of the silicon d-SWSs [15]. During this metal-assisted chemical etching process, the Ag sank into the silicon substrate through a chemical reaction of locally induced excessive oxidation and dissolution of silicon underneath the Ag mesh structures [13–15]. Thus, the d-SWSs have inversely transferred morphology of the Ag mesh patterns, and the dimensions of d-SWSs rely on the geometry of Ag mesh. The etching direction was identical to the crystallographic orientation of silicon wafer, due to the chemical instability of the (100). Subsequently, the wafers were immersed in nitric acid solution to completely remove the residual Ag and were then rinsed with DI water and dried under a flow of N_2 gas.

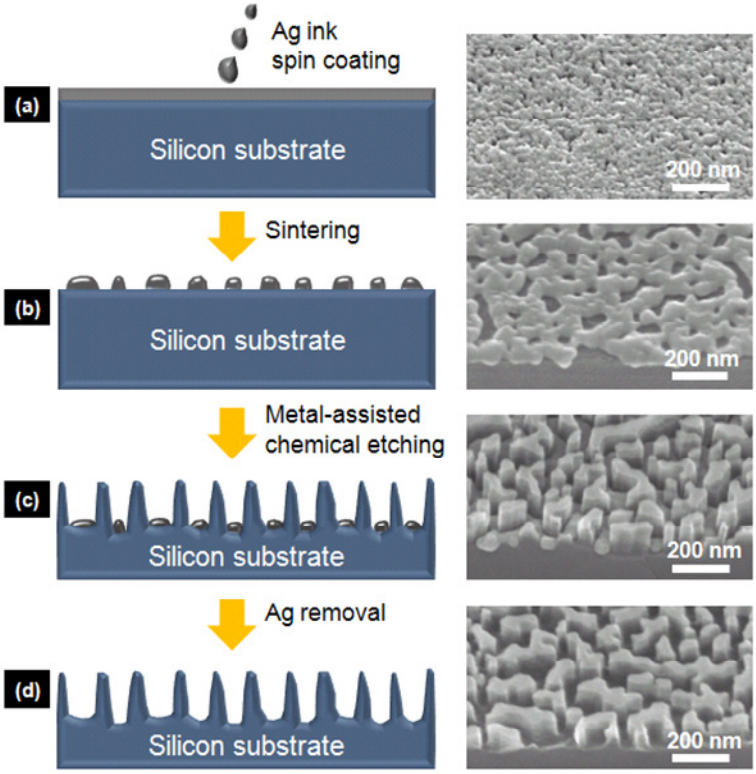

Fig. 1. Schematic illustration (left column) of the process steps for fabricating the d-SWSs by spin-coating Ag ink and metal-assisted chemical etching. Tilted cross-sectional view SEM images (right column) in each process step.

3. Results and discussion

Figure 2(a) exhibits the exposed surface ratio of silicon wafers as a function of sintering temperature. The sintering temperature was carefully adjusted to obtain silicon d-SWSs with

#149230 - $15.00 USD Received 14 Jun 2011; accepted 30 Jun 2011; published 2 Aug 2011

various dimensions because it strongly influenced the geometry of the self-aggregated Ag mesh as well as antireflection properties of SWSs [3]. To analyze the exposed surface area, a commercial image processing program (ImageJ 1.42q, NIH) was utilized. As the sintering temperature increases, the exposed surface ratio gradually increases, which is attributed to agglomeration of Ag to minimize the surface free energy, when the surface energy of Ag is sufficient for thermal dewetting [10]. As shown in the insets in Fig. 2(a), both the interspace (dark contrast regions) between the adjacent Ag mesh (gray contrast regions) and the dimensions of the Ag mesh increases, when the sintering temperature increases. Figure 2(b) shows top view SEM images of the d-SWSs after metal-assisted chemical etching for 10 min. In the SEM images, the gray contrast regions show the surface of SWSs, and the dark contrast regions show the etched silicon regions. The SEM images are evidence of the formation of the d-SWSs with different dimensions by adjusting the sintering temperature.

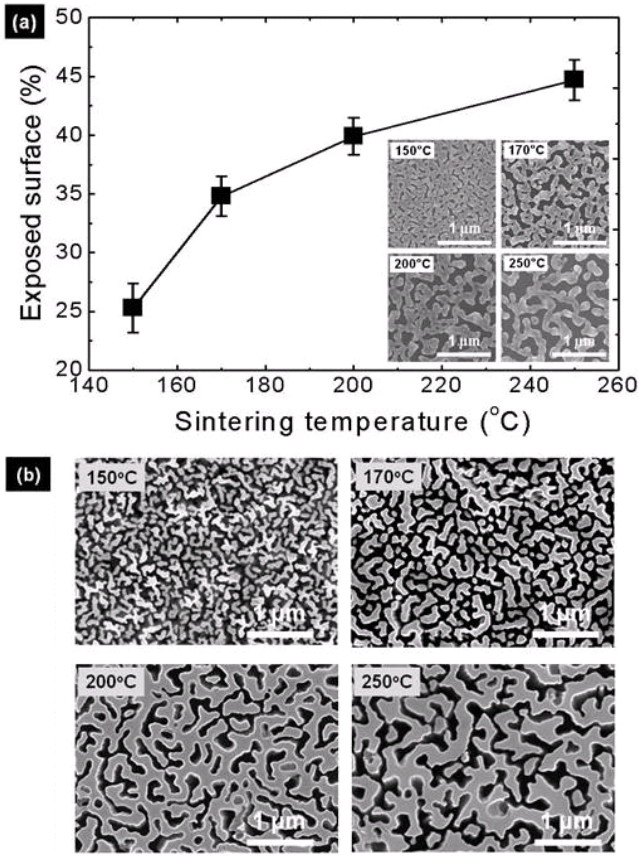

Fig. 2. (a) Exposed surface ratio of silicon wafers as a function of sintering temperature. The insets show top view SEM images of Ag mesh structure (gray contrast region). (b) Top view SEM images of d-SWSs after metal-assisted chemical etching process for 10min.

The reflectance spectra of the fabricated d-SWSs by using metal-assisted chemical etching were measured using a UV-VIR-NIR spectrophotometer (Cary 5000, Varian) equipped with an integrating sphere for hemispherical reflectance measurement. Figure 3 shows the sintering temperature dependent hemispherical reflectance spectra as a function of wavelength of 300-1100 nm for the 10 min etched d-SWSs. The reflectance of bare silicon is also shown as a reference. The bare silicon exhibits more than 30% hemispherical reflectance, whereas the d-SWSs remarkably reduce reflectance throughout the entire wavelength range. The d-SWSs with small dimensions (150°C) exhibit low reflectance at narrow, short wavelength regions,

#149230 - $15.00 USD Received 14 Jun 2011; accepted 30 Jun 2011; published 2 Aug 2011

whereas the d-SWSs with larger dimensions (200°C and 250°C) exhibit stable reflectance at broad long wavelength regions. This behavior is attributed to broaden and shift to higher wavelengths of the low reflectance region by increasing the dimension of SWSs [3]. Among the d-SWSs, the d-SWSs with a 170°C sintering temperature displays the best broadband antireflection capability with an average hemispherical reflectance of 1.57% in the wavelength range of 300-1100 nm, due to its mixed SWSs dimensions changing from 150°C to 200°C. The rapid increase of reflectance spectra at wavelength longer than 1050 nm is due to the scattered light from the back surface.

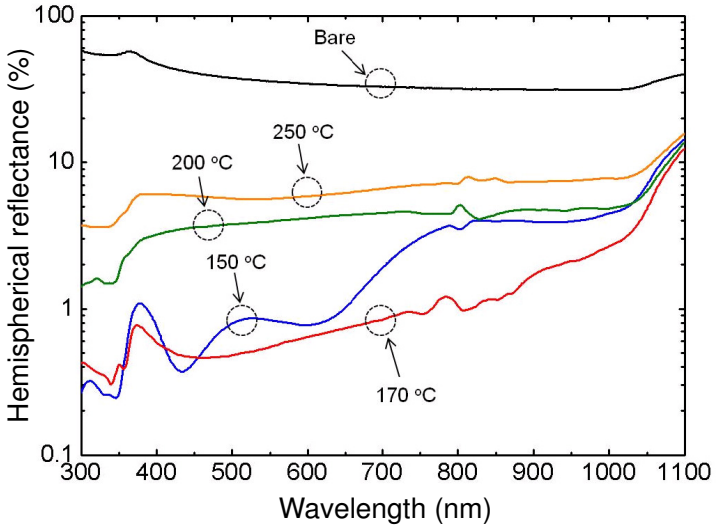

Fig. 3. The measured hemispherical reflectance spectra as a function of wavelength for the fabricated d-SWSs with an etching time of 10 min.

Figure 4(a) shows the etching depth as a function of etching time, and the insets show the cross-sectional SEM images of the fabricated d-SWS with a sintering temperature of 170°C for various etching times. The etching depth increases linearly with etching time at an approximate rate of 44.3 nm/min. This result means that the silicon SWSs with tailored height can be obtained by controlling the etching time. Figure 4(b) shows the solar-weighted reflectance (SWR) as a function of etching time for various sintering temperatures. The SWR is an important parameter for the optimization of the antireflection structure for solar cells, and it can be explained as the ratio of reflected photons to total incident photons, i.e., the normalization of reflectance spectra with the terrestrial air mass 1.5 global (AM1.5G) as given in following equation [16]

$$SWR = \frac{\int R(\lambda) N_{photon}(\lambda) d\lambda}{\int N_{photon}(\lambda) d\lambda} \quad (1)$$

where $R(\lambda)$ is the hemispherical reflectance and N_{photon} is the photon number of AM1.5G per unit area per unit wavelength [17]. The calculated SWRs of the d-SWSs are drastically decreased compared to those of bare silicon of 35.91% in the wavelength range of 300-1100 nm. As etching time increases, the SWRs gradually decrease due to a slower change of the effective refractive index between silicon and air, which is due to the increase in height. Although taller height d-SWSs have a smaller SWR, the d-SWSs with lower height are required for practical solar cell applications due to their fragile nature. Therefore, the wafer with a sintering temperature of 170°C and an etching time of 10 min has the lowest SWR of 1.23% and the most appropriate one for silicon solar cell applications.

#149230 - $15.00 USD Received 14 Jun 2011; accepted 30 Jun 2011; published 2 Aug 2011

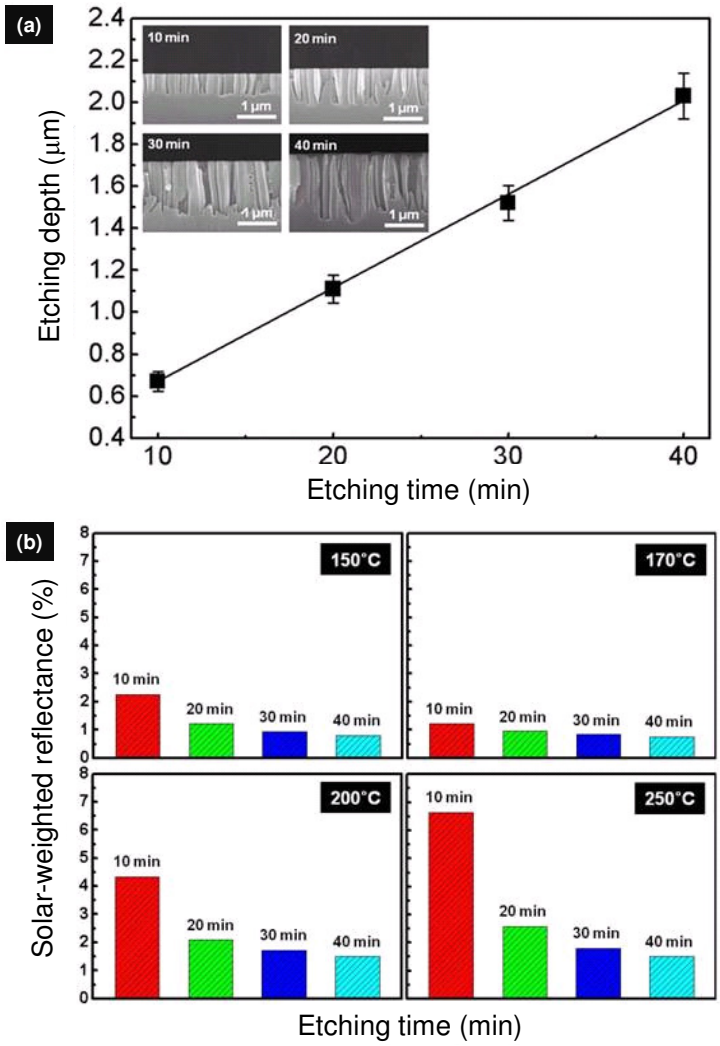

Fig. 4. (a) The etching depth of silicon wafers as a function of etching time, the gradient of the line is about 44.3 nm/min. (b) The calculated SWR of silicon wafers with SWSs as a function of sintering temperatures and etching time.

The angle-dependent antireflection property is also an important parameter to optimize the antireflection structure for improving the performance of optical device such solar cells and light-sensitive detectors. Figure 5 shows contour plots of the incidence-angle-dependent reflectance as a function of wavelength range of 300-2500 nm for wafers etched for 10 min at different sintering temperatures producing different dimensions of d-SWSs. The data were obtained using a Cary variable angle specular reflectance accessory in specular mode. The reflectance increases as the angle of incidence (AOI) increases. The average reflectance over the incidence angle range of 20°-70° and the wavelength range of 300-2500 nm are 10.52%, 4.11%, 7.45%, and 8.56% with increasing dimensions (i.e., sintering temperature). When the measured reflectance for each d-SWSs is compared in the view of lower reflectance through broad wavelength region, the d-SWSs with a sintering temperature of 170°C again show the best result, i.e., have the lowest reflectance value in the broad wavelength and average reflectance of <5% up to AOI of 55°. This behavior is attributed to having mixed SWSs dimensions between the smaller SWSs and the larger SWSs, which dominantly reduce

#149230 - $15.00 USD Received 14 Jun 2011; accepted 30 Jun 2011; published 2 Aug 2011

surface reflection in the short wavelength region and long wavelength region, respectively [3,4].

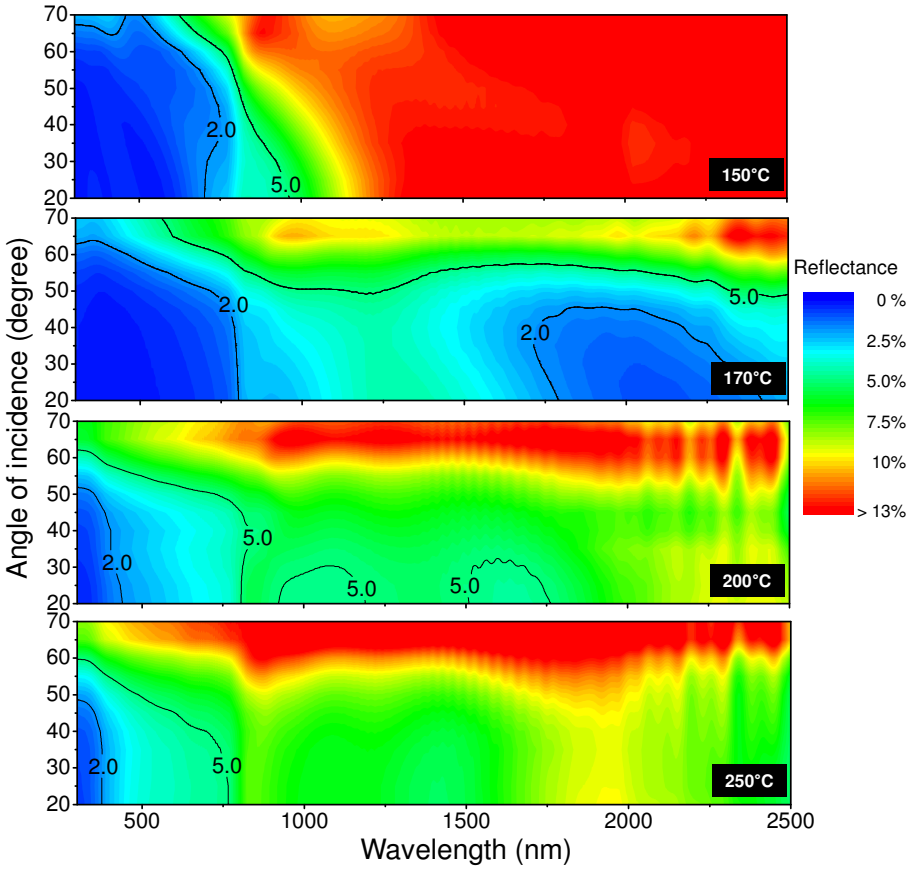

Fig. 5. Incidence-angle-dependent reflectance as a function of wavelength for 10 min etched silicon SWSs with various sintering temperatures.

Figure 6(a) shows fabricated 4-inch d-SWSs (black silicon) with a sintering temperature of 170°C and bare silicon for comparison of background image reflection. The black silicon does not reflect anything because of its excellent antireflective characteristics, while the bare silicon reflects the background image. To investigate the surface uniformity of the wafer-scale processed black silicon, a white light source (halogen lamp) surface mapping system (RPM 2000, Accent) was used. The color in Fig. 6(b) and 6(c) represent the surface reflection intensity of the bare and the black silicon. The reflected intensity of the black silicon is significantly lower than that of the bare silicon, and has a good surface uniformity. Consequently, the nanofabrication technique using Ag ink and metal-assisted chemical etching easily produces wafer-scale broadband antireflective black silicon for optical applications. Recently, this metal-assisted chemical etching mechanism has also been utilized to fabricate microstructures or nanoporous structures on III-V compound semiconductor materials, such as GaAs and GaN [18,19], which have been widely used for optoelectronic device applications. Thus, this technique could also be utilized to fabricate high-efficiency III-V material based optical devices.

#149230 - $15.00 USD Received 14 Jun 2011; accepted 30 Jun 2011; published 2 Aug 2011

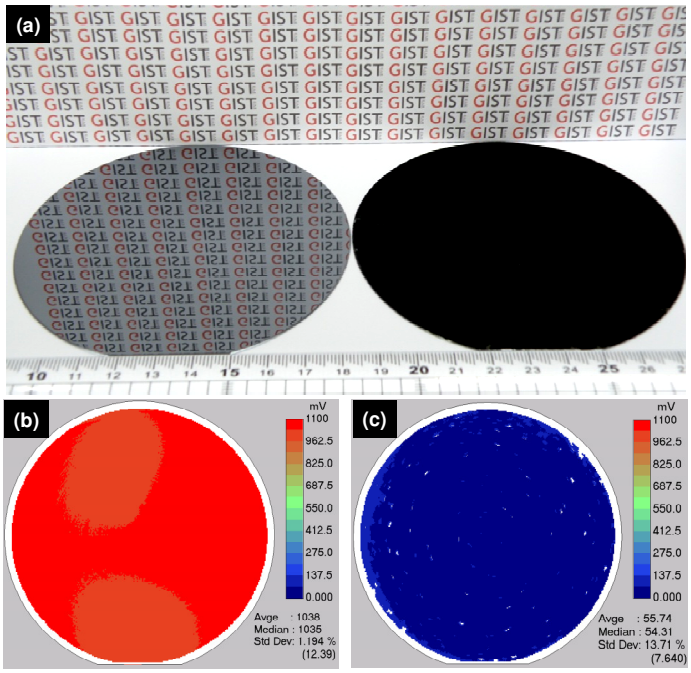

Fig. 6. (a) Comparison of 4-inch processed antireflective black silicon (right) with reflective polished bare silicon (left). (b) Surface map of bare silicon wafer. (c) Surface map of black silicon wafer.

4. Conclusion

We fabricated wafer-scale broadband antireflective silicon d-SWSs by using a simple and low-cost nanofabrication method that uses spin-coating Ag ink and metal-assisted chemical etching. To achieve desirable antireflective structure for practical device applications, d-SWSs with various dimensions were fabricated by changing the sintering temperature of the spin-coated Ag ink. The fabricated 4-inch silicon d-SWSs showed significantly lower reflection values compared to bare silicon, and their antireflection properties were strongly related to the dimensions of the d-SWSs. The black silicon with the most appropriate d-SWSs (i.e., 170°C sintering temperature and 10 min etching time) for practical solar cell application exhibited a SWR value of 1.23% in the wavelength range of 300-1100 nm and an average reflectance value of <5% up to AOI of 55° in the wavelength range of 300-2500 nm, as well as good surface uniformity. The proposed nanofabrication method provides the fabrication of well-tailored antireflective d-SWSs by controlling the sintering temperature of Ag ink (SWSs dimensions) and etching time (SWSs height). Furthermore, it may also provide a promising potential for high-efficiency optical and optoelectronic device applications.

Acknowledgements

This work was supported by the National Research Foundation of Korea (NRF) grant funded by the Korea government (MEST) (No. 2011-0017606).

#149230 - $15.00 USD Received 14 Jun 2011; accepted 30 Jun 2011; published 2 Aug 2011